Developing Parasitic Cancellation Technologies to Improve EMI Filter Performance for Switching Mode Power Supplies

Shuo Wang, *Student Member, IEEE*, Rengang Chen, *Student Member, IEEE*, Jacobus Daniel Van Wyk, *Fellow, IEEE*, Fred. C. Lee, *Fellow, IEEE*, and Willem Gerhardus Odendaal, *Member, IEEE*

***Abstract*—Electromagnetic interference (EMI) filters have been used for power electronics converters to attenuate switching noise and meet EMI standards for a long time. However, because of the parasitics in the filters, filters cannot attenuate high-frequency noises efficiently. In this paper, critical parasitics, which include both mutual and self-parasitics, are first identified in both differential and common mode filters. Three techniques are then developed to cancel the adverse effects of mutual parasitics. These techniques can effectively cancel the inductive couplings between an inductor and capacitors, between an inductor and trace loops, and between two capacitors. Two additional techniques are further developed to cancel the self-parasitics of components, such as the equivalent series inductance of capacitors and the equivalent parallel capacitance of inductors. Experiments are carried out to verify these developed techniques. It is shown that the high-frequency performance of EMI filters is drastically improved.**

***Index Terms*—Electromagnetic interference (EMI) filter, equivalent parallel capacitance (EPC), equivalent series inductance (ESL), parasitic cancellation, parasitic coupling, self-parasitics.**

I. Introduction

In power electronics applications, the electromagnetic (EMI) filter is a necessary interface between the power line and power supplies. The ac/dc and dc/dc converters in power systems work in switching mode. They generate conducted switching noise with a spectrum that ranges from the used switching frequencies to 30 MHz. EMI standards, such as EN55022 class A, specify the frequency range (150 kHz–30 MHz) and noise limit that power supplies need to meet. To satisfy these EMI standards, one or two stages of EMI filters are usually needed. A typical one-stage EMI filter used in power supplies is shown in Fig. 1.

In Fig. 1, C_{Y1} and C_{Y2} are common mode (CM) capacitors and their values are equal. C_1 and C_2 are differential mode (DM) capacitors. Inductor $L_{\rm CM}$ is a CM inductor and $L_{\rm DM}$ is a DM inductor. Fig. 2 shows the traditional structure of a CM and DM inductor. Two windings are wound on the two sides of a high micrometer and high-loss ferrite toroidal core. The coupling polarities are shown Fig. 2. The magnetic fluxes generated by the CM current in the two windings have the same magnitude and direction in the core so that the CM inductance $L_{\rm CM}$ is the coupled inductance of the two windings. The magnetic fluxes generated by the DM current in the two windings have the same magnitude but different directions in the core so that the DM inductance $L_{\rm DM}$ is the leakage inductance of the two windings.

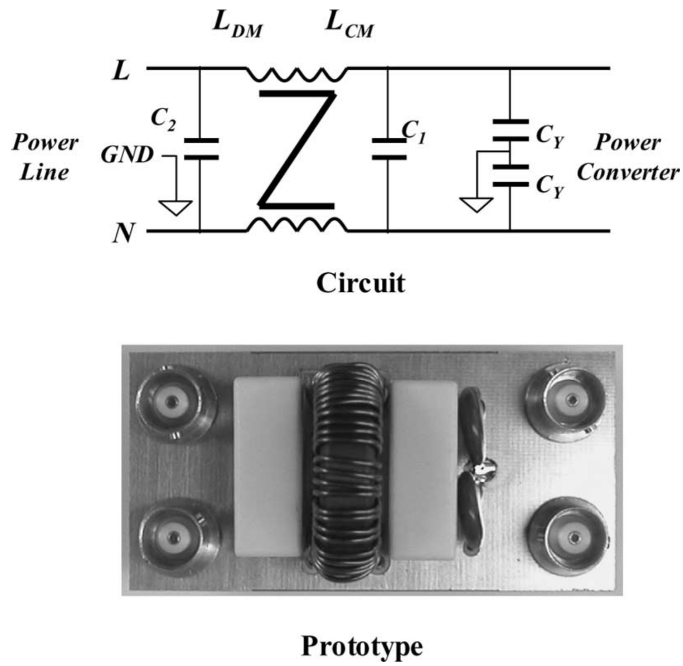

Fig. 1. One-stage EMI filter under investigation.

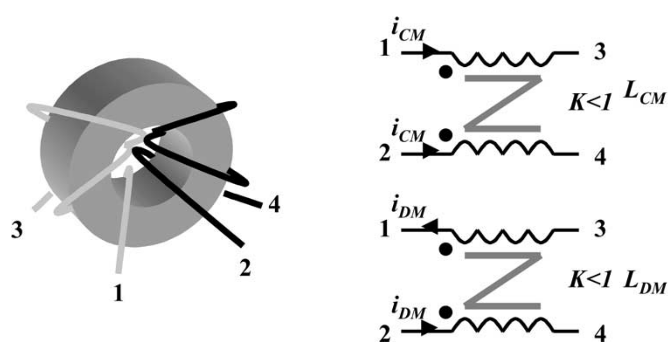

Fig. 2. CM and DM inductor of the filter.

It is well known that there are two types of parasitic parameters in circuits: self-parasitics and mutual parasitics. The self-parasitics of components, such as equivalent inductance

Manuscript received February 1, 2005; revised July 4, 2005.

S. Wang, J. D. van Wyk, F. C. Lee, and W. G. Odendaal are with the National Science Foundation Engineering Research Center for Power Electronics Systems, the Bradley Department of Electrical and Computer Engineering, Virginia Polytechnic Institute and State University, Blacksburg, VA 24061 USA.

R. Chen is with International Rectifier, EI Segundo, CA 90245 USA.

Digital Object Identifier 10.1109/TEMC.2005.857367

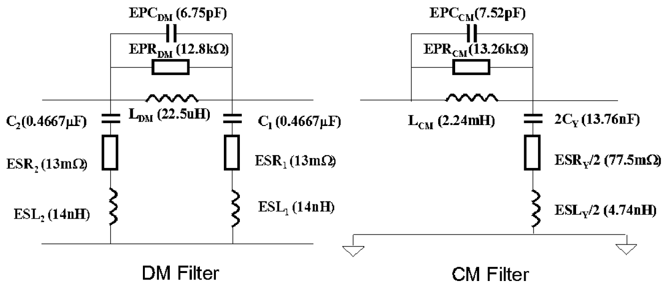

Fig. 3. CM and DM filter models including parasitics of components.

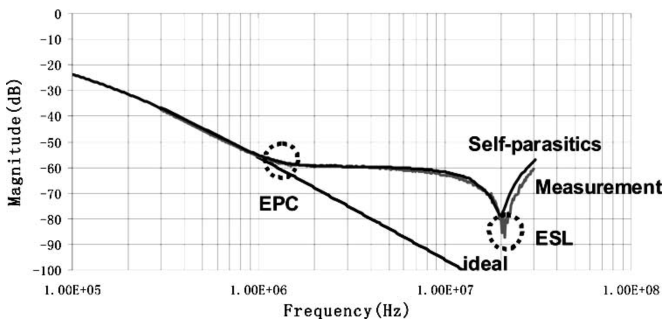

Fig. 4. Comparison of measured and simulated S21 for CM filter.

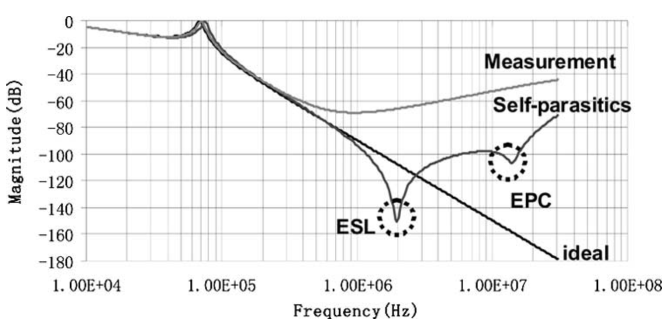

Fig. 5. Comparison of measured and simulated S21 for DM filter.

(ESL) of capacitors and equivalent parallel capacitance (EPC) of inductors, determine the high-frequency performance of components. The mutual parasitics exist between two components, between a component and the printed circuit board (PCB) layouts, and between PCB traces. For a filter prototype shown in Fig. 1, CM and DM filter models considering self-parasitics are shown in Fig. 3. For convenience, CM capacitors are disconnected when the DM filter is modeled using S-parameters. Simulated and measured values of S21 for both CM and DM filters are compared in Figs. 4 and 5.

For the CM filter in Fig. 4, the measured value of S21 matches the simulated value up to 30 MHz. The first corner frequency is generated by the parallel resonance of the CM inductance $L_{\rm CM}$ and the winding capacitance $\rm EPC_{CM}$, and the second corner frequency is generated by the series resonance of the equivalent CM capacitance $2C_Y$ and the equivalent series inductance $\mathrm{ESL}_Y/2$. This indicates that the self-parasitics of components determine the performance of the CM filter. To improve the CM filter's high-frequency (HF) performance, the winding capacitance $\rm EPC_{CM}$ should be reduced. On the other hand, for the

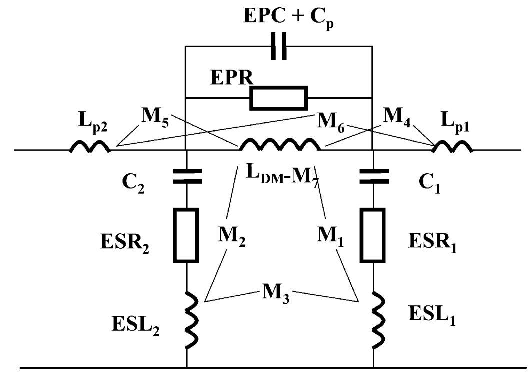

Fig. 6. Parasitic couplings in a DM filter.

DM filter in Fig. 5, the measured value S21 is far away from the simulated value above 400 kHz, which means mutual parasitics determine the HF performance of the DM filter. To improve the DM filter's HF performance, mutual couplings should first be reduced, and then, the ESL should be reduced.

This paper will identify and quantify the parasitic couplings in EMI filters. Technologies are developed to control mutual parasitics and self-parasitics. Experiments are carried out to prove the developed technologies.

II. Mutual Parasitic Cancellation Technique

As stated in Section I, mutual parasitics are important to DM filters only. Both inductive and capacitive parasitic couplings exist in DM filters. Inductive couplings tend to amplify their effects on the branch that has the smaller current between two branches with a large current difference. The inductive couplings, such as those between capacitor branches and the inductor branch, between two capacitor branches, between in-and-out trace loops, and between inductor and in-and-out trace loops are therefore important parasitic couplings. At the same time, capacitive couplings tend to amplify their effects on the node that has the lower potential between two nodes with a large potential difference. The capacitive coupling between in-and-out traces is thus an important coupling. All these parasitic couplings are shown in Fig. 6 [3]. They can be divided into six categories as follows:

1) inductive coupling between inductor and capacitors: M_1 and M_2;
2) inductive coupling between inductor and trace loops: M_4 and M_5;
3) inductive coupling between two capacitors: M_3;
4) inductive coupling between in-and-out trace loops: M_6;
5) inductive coupling between ground plane and inductor: M_7;
6) capacitive coupling between in-and-out traces: C_p.

In Fig. 6, M_7 represents the effects of induced eddy currents in the ground plane on the DM inductance. Because it is much smaller than the DM inductance [4], it can be ignored. Furthermore, because of the low impedances of the two capacitor branches, the effects of C_p are ignored. M_6 represents the inductive coupling between in-and-out trace loops. M_6 can be minimized by simply reducing in-and-out trace loop areas.

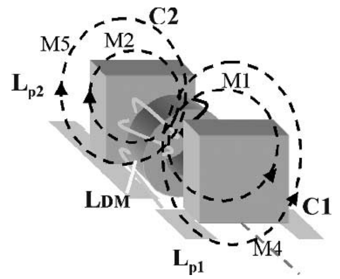

Fig. 7. Inductive couplings between the inductor and capacitors.

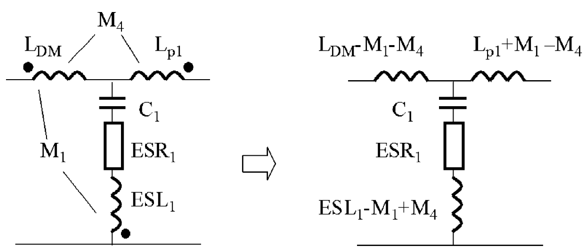

Fig. 8. Effects of mutual inductances on capacitors.

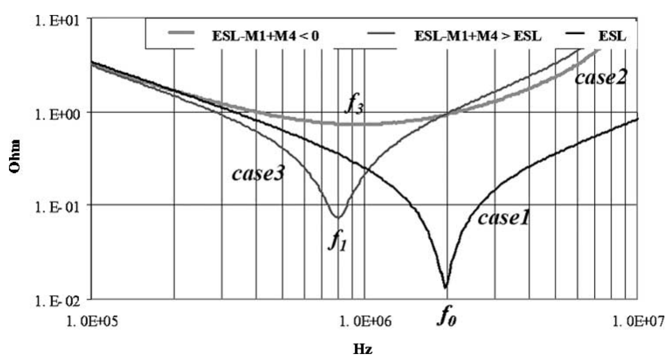

Fig. 9. Effects of mutual inductances on the impedances of capacitors.

A. *Reducing* M_1, M_2, M_4*, and* M_5

Because the DM inductance is the leakage of the two windings, the DM magnetic fluxes generated by the DM current extend to the air and easily couple to other components and traces. M_1, M_2, M_4, and M_5 are illustrated in Fig. 7. Magnetic fluxes link the currents in capacitors C_1 and C_2 to generate M_1 and M_2 and link the currents in trace loops L_{p1} and L_{p2} to generate M_4 and M_5. Depending on the winding directions of the inductor, the polarities of these couplings are different. Effects of M_1 and M_4 on the impedance of capacitor C_1 are illustrated in Fig. 8. The impedances of C_1 with and without effects of M_1 and M_4 are shown in Fig. 9. In Fig. 9, case 1 is the measured impedance of a single capacitor C_1. Case 2 is the extracted impedance of the capacitor C_1 branch with the effects of M_1 and M_4, when the inductor has winding direction 1. Case 3 is the extracted impedance of capacitor C1 branch with the effects of M_1 and M_4, when the inductor has winding direction 2. In Fig. 9, f_0 is the self-resonant frequency of the capacitor; f_1 is the series resonant frequency when $M_4 - M_1 > 0$; f_3 is the minimum impedance frequency of the capacitor branch when $M_4 - M_1 < 0$ and $|M_4 - M_1| >$ ESL; f_3 is different from the resonant frequencies because no phase polarity change occurs [4]; f_0, f_1, and f_3 are given by (1)–(3) as follows:

$$f_0 = \frac{1}{2\pi\sqrt{\mathrm{ESL} \times C}} \tag{1}$$

$$f_1 = \frac{1}{2\pi\sqrt{(\mathrm{ESL} - M_1 + M_4)C}} \tag{2}$$

$$f_3 = \frac{1}{2\pi\sqrt{(-M_1 + M_4 - \mathrm{ESL})C}}. \tag{3}$$

In Fig. 8, L_{p1} is approximately 40 nH. L_{DM} is 22.5 μH for case 2, and 18.91 μH for case 3. Mutual inductances M_1 and M_4 are extracted through measurements by comparing f_1 and f_3 with f_0 [3]. The results are the following: M_1 is 89.3 nH, and M_4 is 18.7 nH for case 2; M_1 is -83.3 nH, and M_4 is -10.3 nH for case 3. Because M_1 and M_2 are much larger than M_4 and M_5, it is concluded that M_1 and M_2 make the performance of the two capacitors much worse than expected.

To reduce the net magnetic fluxes linking the capacitors and trace loops, Fig. 10 shows the proposed rotation of the inductor windings by 90° [4]. M_1 is then reduced to only 7.5 nH in the experiment [3]. The improvements of this method on capacitor impedance and filter performance are shown in Figs. 11 and 12. In Fig. 11, case 4 is the impedance of the capacitor with 90° rotated windings, which is much lower than those with winding direction 1 and winding direction 2 above 1 MHz. As a result, the S21 of the filter in Fig. 12 is better than the values for the other two above 1 MHz.

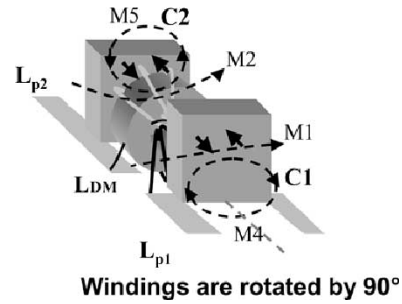

Fig. 10. Rotating windings by 90° to reduce the inductive couplings.

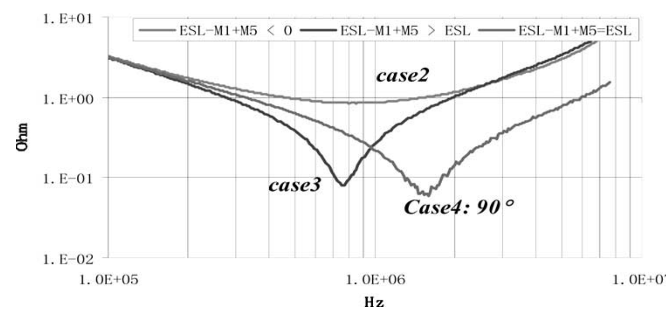

Fig. 11. Improvement of the impedances of capacitors.

B. *Reducing* M_3

Fig. 13(a) shows capacitors C_1 and C_2 on the filter PCB. The magnetic flux Φ_{M3} produced by the current I_1 in capacitor C_1

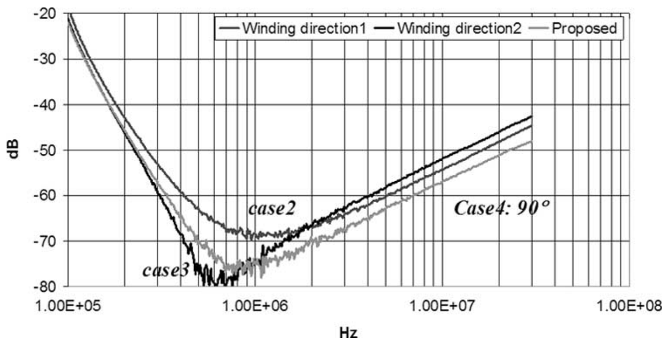

Fig. 12. Improvement of the filter performance.

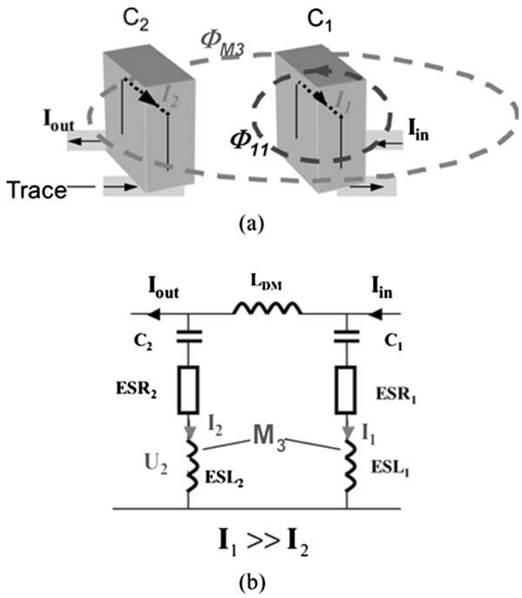

Fig. 13. Inductive coupling between two DM capacitors. (a) Mutual inductance between two capacitors. (b) Equivalent circuit including $L_{\rm DM}$ and M_3.

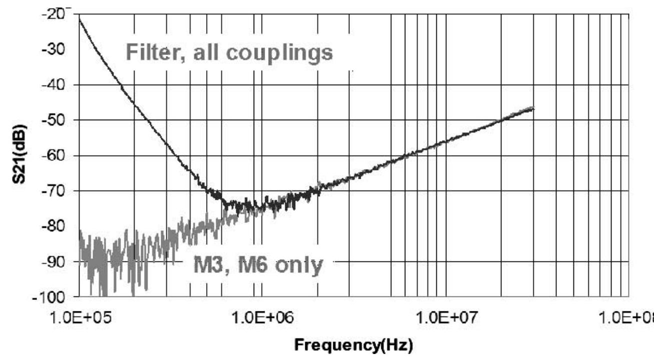

Fig. 14. Mutual inductance between two capacitors determines filter HF performance.

links the current I_2 in capacitor C_2. The mutual inductance M_3 is therefore defined by (4). Then, the equivalent circuit including $L_{\rm DM}$ is shown in Fig. 13(b). In Fig. 13(b), because most of the input HF noise current is bypassed by C_1, I_1 is much larger than I_2. The voltage U_2 on ESL_2 and the effects of M_3 can be described by (5) and (6). From (5) and (6), effects of M_3 are amplified by $|I_1/I_2|$ times and, as a result, a very small inductive coupling between the two capacitors can induce a significant voltage.

$$\mathbf{M_3} = \frac{\Phi_{M3}}{I_1} \tag{4}$$

$$\mathbf{U}_2 = j\omega\mathbf{I}_2\left(\mathrm{ESL}_2 + \frac{\mathbf{I}_1}{\mathbf{I}_2}M_3\right) \tag{5}$$

$$\text{if } \left|\frac{\mathbf{I}_1}{\mathbf{I}_2}\right| > \frac{\mathrm{ESL}_2}{M_3}, |L_{\rm eq}| = M_3 \times \left|\frac{\mathbf{I}_1}{\mathbf{I}_2}\right| > \mathrm{ESL}_2. \tag{6}$$

Two measurements are carried out in Fig. 14. For the first measurement, S21 of the filter with proposed rotated inductor windings is measured. For the second measurement, the inductor is disconnected from the circuit (but still kept on the PCB because the inductor core affects the magnetic field distribution), and then, S21 of the circuit is measured. For the second measurement, because the inductor is disconnected, from Fig. 6, only M_3 and M_6 are left in the filter. Comparing the S21 of the two experiments, the values of S21 are exactly the same above 1 MHz; therefore, after inductor windings are rotated by 90°, HF noise current propagates through M_3 and M_6 instead of through the inductor. This means that effects of the inductor can be ignored above 1 MHz if the proposed rotated inductor windings are used. M_6 can be easily minimized by reducing the in-and-out trace loop areas. So, M_3 is the critical mutual coupling that should be minimized.

To reduce M_3, it is proposed that the two capacitors should be located perpendicularly. Parasitic extraction shows the method can reduce M_3 from 249 pH to 83 pH, which is a significant $2/3$ reduction. Unlike the capacitor orientations in Figs. 7 and 10, the perpendicular capacitors cannot minimize both M_1 and M_2, which are the couplings between the inductor and two capacitors, by rotating the inductor windings, because the related magnetic fluxes cannot be minimized simultaneously. Because of this, a second method that employs a capacitor with an integrated cancellation turn is proposed in Fig. 15.

In Fig. 15(a), a cancellation inductor L_M is integrated with capacitor C_2. L_M has mutual inductance M_A with C_1 and M_B with C_2. The equivalent circuit of these couplings is shown in Fig. 15(b). In the equivalent circuit, U_S is the source voltage and U_L is load voltage. If M_A equals M_3, then U_L is zero. The effects of M_3 are actually canceled. The implementation of L_M is shown in Fig. 16. A three-quarters-turn copper foil is integrated with the film capacitor C_2 (Philips, MKP 0.47 uF/400 V), which forms a three-terminal device. Three terminals of the device correspond to those in Fig. 16. Φ_{M3} is the magnetic flux generated by C_1 links C_2. Φ_{MA} is the magnetic flux generated by C_1 links L_M. If the cancellation turn is designed to make Φ_{M3} equal Φ_{MA}, then M_A is equal to M_3. To achieve this, L_M should be as close to the film roll of C_2 as possible. This guarantees that the cancellation turn is exposed to a similar external magnetic field distribution as the capacitor. Second, the cancellation turn should cover the side and upper edges of the film roll. Most of the flux that links the capacitor also links the cancellation turn. Third, because the HF current propagates

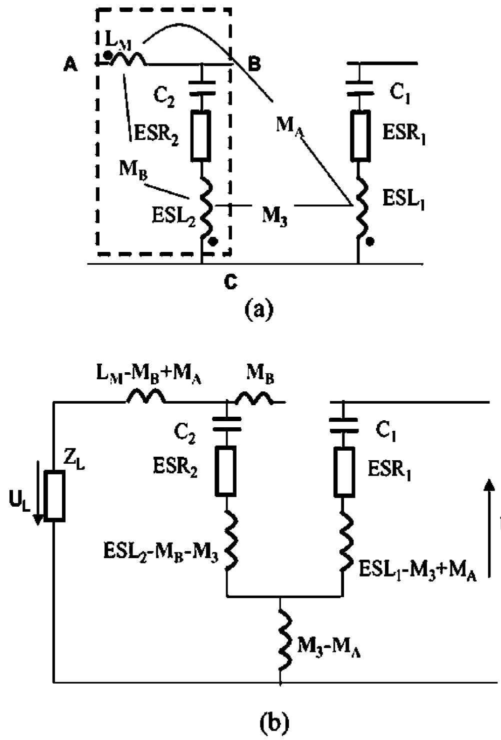

Fig. 15. Using cancellation turn to cancel the inductive coupling between two capacitors. (a) Introducing a cancellation turn (b) Equivalent circuit.

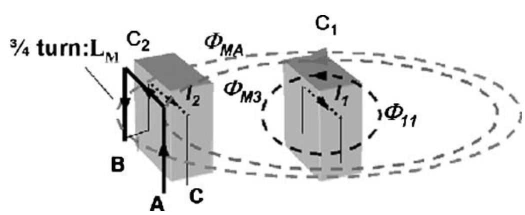

Fig. 16. Integrating cancellation turn with capacitor to cancel M_3.

through the inner edge of the copper foil turn, the coupling area of the cancellation turn is determined by the area enclosed by the inner edge. Finally, the optimal area of the cancellation turn is tuned by conducting experiments. An additional benefit of the cancellation turn is the reduction of the ESL of capacitor C_2, as shown in Fig. 15(b).

Fig. 17 shows the comparison of extracted impedances of M_3. The noise below 1 mΩ is the result of the noise floor of the network analyzer. For the original filter (baseline), M_3 is 249 pH. It is reduced to 89 pH after two capacitors are arranged in a perpendicular fashion. When the integrated capacitor with cancellation turn is used, M_3 is only 19 pH, which is a 92.4% reduction. For the ESL of C_2, parasitic extraction shows that the cancellation turn reduced it from 12 nH to only 4 nH, which is a 67% reduction. The final performance of the filter is compared in Fig. 18. Three curves for S21 are compared in Fig. 18. The baseline case is the filter without a cancellation turn and without 90° rotated windings. When the inductor windings are rotated by 90°, the filter has about a 5-dB improvement, as the second curve shows. If the two capacitors are arranged in

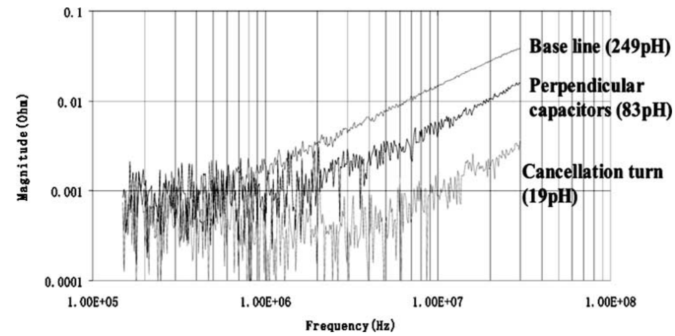

Fig. 17. Extracted impedances of M_3.

a perpendicular fashion, there is a 20-dB improvement above 3 MHz, which is what the third curve shows. The final case is the filter with 90° rotated windings and the capacitor with an integrated cancellation turn. The S21 is indeed below the noise floor of the network analyzer above 1 MHz. The cancellation of M_1, M_2, M_3, M_4, M_5, and the ESL of capacitor C_2 results in a factor-of-100 improvement (40 dB) in filtering performance at 30 MHz. The noise in Fig. 18 is the noise floor of the network analyzer.

C. Two-Stage EMI Filter

For the two-stage DM EMI filter shown in Fig. 19, because of the large current difference between C_1 and C_3, the inductive couplings between C_1 and C_3 determine the HF performance of the filter [3]. It is similar to that in a one-stage EMI filter. This coupling should be canceled to improve filter performance. A capacitor with an integrated cancellation turn then replaces C_1 in the filter. Windings of the two inductors are also rotated by 90°. Fig. 20 shows a comparison of the filter performance. The baseline case is the S21 of the filter without taking any measures. The second case is the filter with the 90° rotated windings and the capacitor with an integrated cancellation turn. Compared with the baseline, the performance is improved from -60 dB to below -90 dB. More than 30-dB improvement is achieved at 30 MHz. Parasitic extraction shows that mutual inductance between C_1 and C_3 reduced from 110 to 14 pH—an 87% reduction. The cancellation turn can also cancel the couplings between C_1 and C_2 and between C_1 and the inductors, although these are not as important as the coupling between C_1 and C_3.

Because the cancellation turn already cancels mutual inductance between C_1 and C_3, only one capacitor with an integrated cancellation turn is needed on the sides of the filter. For the EMI from the outside the filter, it is also expected that the cancellation turn can at least partly cancel the effects on the capacitors because of the opposite coupling polarities between the capacitor and the cancellation turn.

III. Self-Parasitic Cancellation Technique

Just as stated in Section I, if mutual parasitics are minimized, for the DM filter, the ESL of capacitors should be canceled, and for the CM filter, the EPC of inductors should be canceled to further improve filter performance.

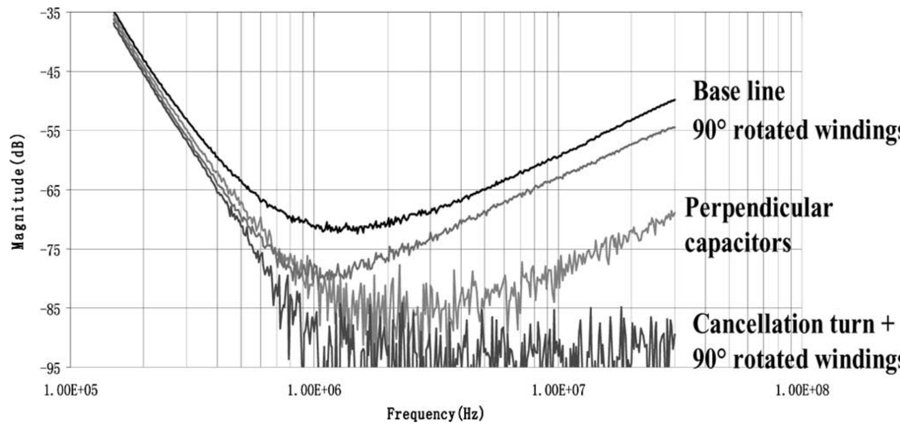

Fig. 18. Comparison of filter performance.

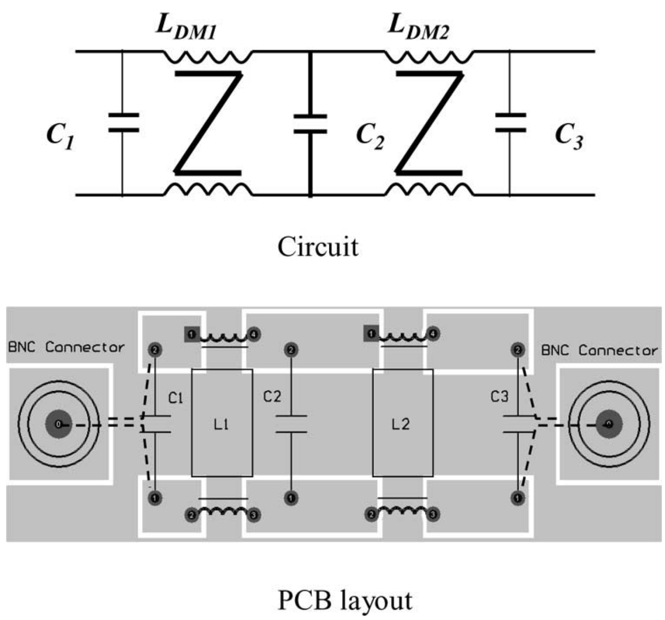

Fig. 19. Two-stage DM filter and PCB layout.

A. Cancellation of Equivalent Series Inductance (ESL)

Above the series resonant frequency of the ESL and the capacitance, a capacitor behaves like an inductor. To improve the capacitor HF performance, the ESL must be effectively reduced. Mutual inductance between two winding inductors is introduced in [8] to cancel ESL. Fig. 21 shows a different proposal for ESL cancellation [2].

In Fig. 21(a) and (b), networks 1 and 2 have the same $\mathbf{Z}$ matrix as given in (7). Because they are equivalent, the two networks have the same characteristics as seen from their two ports. Comparing these two networks, the impedances of Z_1 in network 1 are actually subtracted from Z_3, and are pushed to the two sides of the signal paths, as shown in network 2. Based on this observation, the ESL of the two capacitors can be canceled using extra inductors, just as shown in Fig. 21(c) and (d).

$$\mathbf{Z} = \begin{pmatrix} \frac{Z_3+Z_1}{2} & \frac{Z_3-Z_1}{2} \\ \frac{Z_3-Z_1}{2} & \frac{Z_3+Z_1}{2} \end{pmatrix}. \tag{7}$$

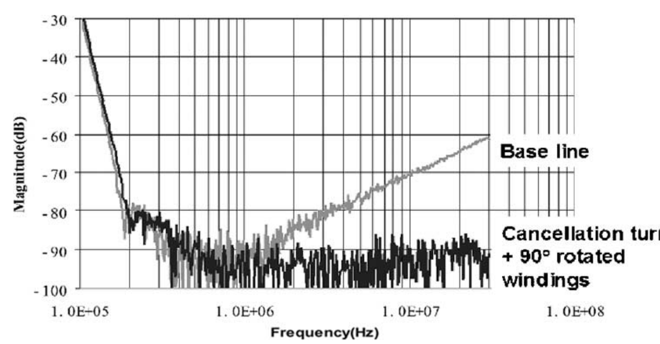

Fig. 20. Comparison of filter performance.

Because the ESL is usually very small, the cancellation inductors can be constructed using PCB windings or a piece of wire. Fig. 22 shows the implementation using one turn of a PCB winding. the whole cancellation structure can be packaged as one four-terminal device. A prototype for two film capacitors (Philips, MKP 0.47 μF/400 V) was built, and the S21 was tested. The prototype is compared with two parallel capacitors in Fig. 23.

Fig. 23 shows that, after the ESL is canceled, a 27-dB improvement is achieved at 30 MHz. For the parallel capacitors, a resonance is caused by the ESL at about 2 MHz; however, after the ESL is canceled, the resonance at 2 MHz disappears. The bump between 10 and 20 MHz on the two curves is caused by the transmission line structure of film capacitors [5], which deteriorates HF capacitor performance; consequently, the ESL cancellation is not as good as expected.

The same technique can also be applied to other types of capacitors such as electrolytic capacitors. A prototype with electrolytic capacitors was built and the S21 measured. Fig. 24 shows the comparison between the prototype and two parallel capacitors. This figure shows that the performance of electrolytic capacitors at 30 MHz is almost the same as it would be at 150 kHz, which implies that electrolytic capacitors can achieve a very good HF performance by using this method. The prototype achieved more than a 27-dB improvement at 30 MHz, compared with the parallel capacitors. Because the self-resonant frequency

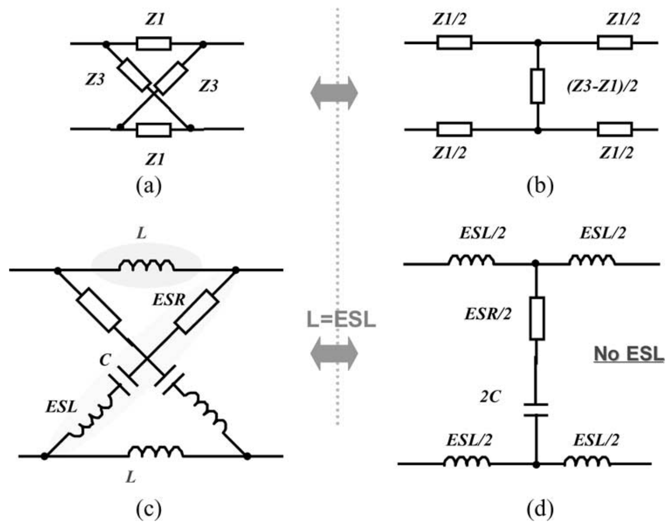

Fig. 21. Illustrating the idea of ESL cancellation. (a) Network 1. (b) Network 2. (c) Two capacitors with two cancellation inductors. (d) Equivalent circuit of ESL cancellation.

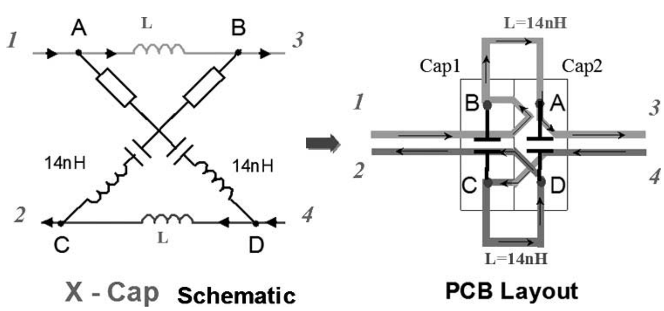

Fig. 22. Implementation of ESL cancellation on PCB.

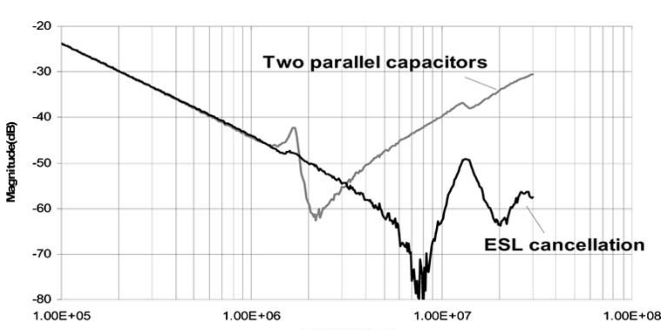

Fig. 23. Comparison of film capacitor (0.47 μF/400 V) performance.

of the investigated electrolytic capacitors is lower than 100 kHz, the curve shape in Fig. 24 is different from the cases in Fig. 23.

The prototype of the film capacitors is used in an L-C EMI filter with minimized mutual parasitics, and then, its S21 is compared with the filter with two parallel capacitors in Fig. 25. Because of the ESL, the case of two parallel capacitors has a resonance at about 2 MHz. However, for the ESL cancellation case, no resonance is observed at about 2 MHz, and the S21 goes down to a higher attenuation as frequency increases. At 30 MHz, a 20-dB improvement is achieved. The proposed technique can be used in other areas besides power electronics.

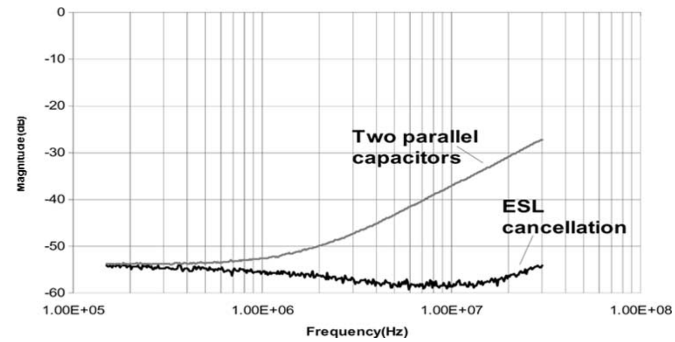

Fig. 24. Comparison of electrolytic capacitor (220 μF/250 V) performance.

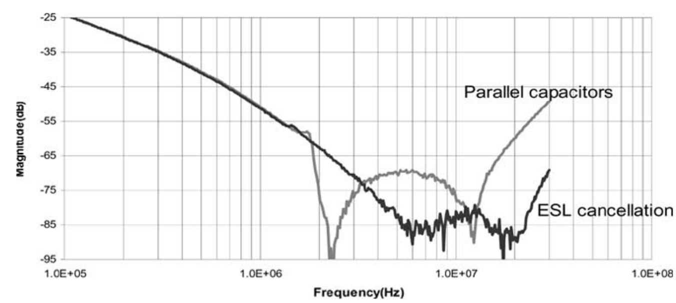

Fig. 25. Comparison of filter performance.

B. Cancellation of Equivalent Parallel Capacitance (EPC)

Because the inductor acts like a capacitor at frequencies above the parallel resonance frequency of the EPC and the inductance, the EPC deteriorates the CM filter HF performance. When not using toroidal cores but planar cores as dictated by the tendency to migrate toward low-profile structures in power electronics [7], this problem became even worse. The EPC must be effectively reduced to improve CM filter HF performance. An extra winding or RF transformer and a capacitor are introduced in [9] to cancel the effects of the winding capacitance. Fig. 26 shows a different idea of EPC cancellation [6].

Fig. 26(a) shows a CM inductor with inductance 4L. If it is center tapped and a grounded capacitor C_2 is connected to its tap as shown in (b), the equivalent circuit can be given by a Π type network, which is shown in (c). The Z_e of the network is given by (8).

$$Z_e = \frac{4j\omega L}{1 + \omega^2 LC_2 - \omega^2 4L \times \text{EPC}} \quad (8)$$

From (8), if C_2 equals 4EPC, then $Z_e = 4j\ \omega L$, so that the circuit is equivalent to a Π type filter without EPC, as shown in (d) [6].

A CM inductor employing planar EE ferrite cores and planar windings is illustrated in Fig. 27(a). Two sets of windings are located in the top two and bottom two windows. Each winding has two layers, and a grounded conductive layer is embedded between the two layers. Each embedded layer has capacitance with two-layer windings, which generates $C_2/2$ and $C_2/4$. The EPC is composed of the capacitances between turns and between the two layers. For CM current, the two sets of windings are closely coupled so that they can be equivalent to the circuit

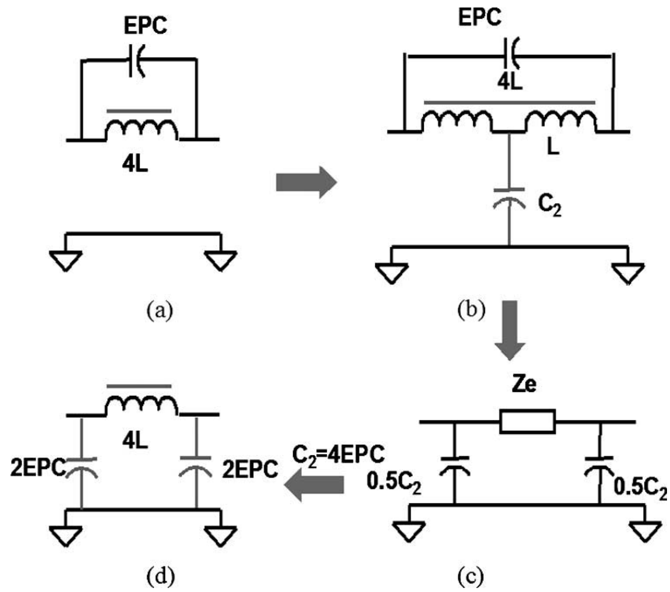

Fig. 26. Illustrating the idea of EPC cancellation. (a) CM inductor with parasitic winding capacitance. (b) Capacitor C_2 is connected to center tap. (c) Equivalent circuit including C_2. (d) EPC is cancelled.

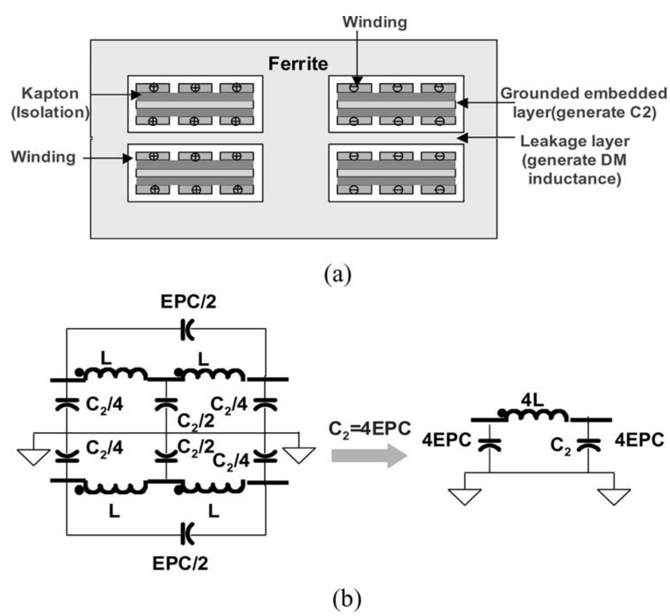

Fig. 27. Implementation of EPC cancellation in a planar inductor. (a) Cross section view of planar inductor. (b) Equivalent circuit of planar inductor.

shown in Fig. 27(b). Designing the areas of embedded layer to make $C_2 = 4\text{EPC}$, the EPC of both sets of windings are canceled. A CM filter, which has the same circuit topology as that in Fig. 1, is built by using the CM inductor prototype and CM capacitors. S21 of the prototype is compared with that without EPC cancellation in Fig. 28. It is shown that the filter performance is improved considerably above 700 kHz. For a filter without EPC cancellation, a parallel resonance of the inductor is observed at about 600 kHz. On the other hand, for the filter with EPC cancellation, no resonance shows up at 600 kHz. The curve of S21 goes down until the series resonance frequency of the CM capacitors occurs. There is about a 30-dB improvement at 30 MHz.

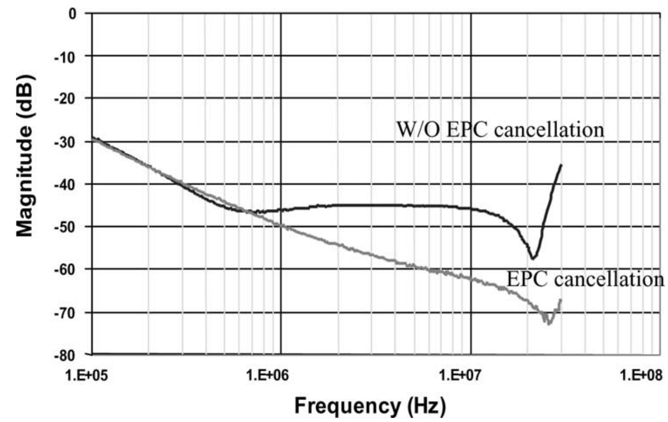

Fig. 28. Comparison of CM filter performance.

IV. Conclusion

This paper first identified the important parasitics in both DM and CM filters. For DM filters, inductive couplings between the two capacitors, between the inductor and the capacitors, and between in-and-out trace loops are critical to HF filter performance. It is proposed that inductor windings are to be rotated by 90° to reduce the couplings between the inductor and the capacitors. Two methods are proposed to reduce the coupling between the two capacitors in the filter. The first one is to orientate the two capacitors perpendicular to each other, and the second one is to integrate a cancellation turn with a capacitor. The second method can also reduce the ESL of the capacitor. It is shown that the proposed methods can be extended to two-stage DM filters. Experiments quantified and verified the proposed methods. It is shown that the developed techniques can considerably improve EMI filter HF performance. For the ESL of capacitors, a method employing a cancellation network is proposed. This network was implemented for both film and electrolytic capacitors to improve filter HF performance. For a CM filter, an approach is proposed to cancel the EPC of the CM inductor. A planar inductor prototype was built to verify experimentally that the approach can greatly improve CM filter HF performance.

References

[1] D. H. Liu and J. G. Jiang, "High frequency characteristic analysis of EMI filter in switch mode power supply (smps)," in *Proc. IEEE Power Electronics Specialists Conf.*, vol. 4, 2002, pp. 2039–2043.

[2] S. Wang, F. C. Lee, and W. G. Odendaal, "Controlling the parasitic parameters to improve EMI filter performance," in *Proc. IEEE Applied Power Electronics Conf.*, vol. 1, Anaheim, CA, 2004, pp. 503–509.

[3] S. Wang, W. G. Odendaal, and F. C. Lee, "Extraction of parasitic parameters of EMI filters using scattering parameters," in *Proc. IEEE Industry Applications Soc. Annu. Meeting*, vol. 4, Seattle, WA, 2004, pp. 2672–2678.

[4] S. Wang, F. C. Lee, D. Y. Chen, and W. G. Odendaal, "Effects of parasitic parameters on EMI filter performance," *IEEE Trans. Power Electron.*, vol. 19, no. 3, pp. 869–877, May 2004.

[5] L. Zhao and J. D. Van Wyk, "A generalized two conductor model for integrated passive components," in *Proc. CPES Seminar 2002*, Blacksburg, VA, pp. 428–433.

[6] R. Chen, J. D. van Wyk, S. Wang, and W. G. Odendaal, "Improving the characteristics of integrated EMI filters by embedded Conductive layers," *IEEE Trans. Power Electron.*, vol. 20, no. 3, pp. 611–619, May 2005.

[7] R. Chen, J. D. van Wyk, S. Wang, and W. G. Odendaal, "Planar electromagnetic integration technologies for integrated EMI filters," in *Proc. IEEE Industry Applications Conf.*, vol. 3, 2003, pp. 1582–1588.

[8] T. C. Neugebauer, J. W. Phinney, and D. J. Perreault, "Filters with inductance cancellation using printed circuit board transformers," *IEEE Trans. Power Electron.*, vol. 19, no. 3, pp. 591–602, May 2004.

[9] T. C. Neugebauer and D. J. Perreault, "Parasitic capacitance cancellation in filter inductors," in *Proc. IEEE Power Electronics Specialists Conf.*, Aachen, Germany, 2004, pp. 3102–3107.

Shuo Wang (S'03) received the B.S.E.E. degree from Southwest Jiaotong University, Chengdu, China, in 1994, the M.S.E.E. degree from Zhejiang University, Hangzhou, China, 1997, and the Ph.D. degree from Virginia Polytechnic Institute and State University (Virginia Tech), Blacksburg, VA, in 2005.

Since 2005, has been a research Assistant Professor with the Center for Power Electronics Systems (CPES), a National Science Foundation engineering research center at Virginia Tech. From 1997 to 1999, he was with ZTE Telecommunication Corporation, Shenzhen, where he was a senior R&D engineer and responsible for the development and support of the power supply for wireless products. In 2000, he worked at UTstarcom Telecommunication Corporation, Hangzhou, where he was responsible for the development and support of the optical access networks.

Dr. Wang received excellent R&D engineer award in 1998 and has one U.S. patent pending.

Rengang Chen (S'01) received the B.Eng. degree of electrical engineering from Huazhong University of Science and Technology, Wuhan, China, and the M.S. degree of electrical engineering from Shanghai Jiao Tong University, Shanghai, China, in 1994 and 1997, respectively. Since 1999, he has been a Ph.D. student and a graduate research assistant in Center for Power Electronics Systems (CPES), Virginia Polytechnic Institute and State University Blacksburg, where he received the Ph.D. degree in electrical engineering in 2004.

He has published more than 20 IEEE conference/transaction papers during his Ph.D. study. He joined International Rectifier as a rotation engineer after his graduation. His research interests include power passive integration and packaging, magnetic component modeling and design, EMI filter design, and modeling and power electronic circuits.

Jacobus Daniel van Wyk (F'90) received the M.Sc.Eng. degree from the University of Pretoria, Pretoria, South Africa, in 1966, the Dr.Sc.Tech. (cum laude) degree from the Technical University, Eindhoven, the Netherlands, in 1969, and the D.Sc. (Eng) (honoris causa) degree from the University of Natal, Natal, South Africa, in 1996.

He worked with the S.A. Iron and Steel Corporation, the University of Pretoria, and the technical and scientific staff of the University in Eindhoven between 1961 and 1971. From 1971 to 1995, he was a chaired Professor of electrical and electronic engineering at the Rand Afrikaans University, Johannesburg, holding chairs in electronics and in power electronics until 1992. He founded the Industrial Electronics Technology Research Group in the Faculty of Engineering in 1978 and directed this unit until 1999. Since July 1995, he has held a special University Council Research Chair in Industrial Electronics at the Rand Afrikaans University; since 2000, he has been in a part-time capacity. He joined the Bradley Department of Electrical and Computer Engineering, Virginia Polytechnic Institute and State University, Blacksburg, in January 2000, where he is the J. Byron Maupin Professor of Engineering. At Virginia Tech, he is in the National Science Foundation Engineering Research Center for Power Electronics Systems, where he leads the High Density Integration Research Thrust. He has worked and published in the fields of semiconductors, microelectronics, electric materials, electromechanical energy conversion, electric drives, power electronics, industrial electronics, control, alternative energy systems, electric vehicles, and many diverse applications in industry, mining, transportation, and electrical energy supply systems. His present research interest is in integrated electronic power processors.

Dr. van Wyk is a Fellow of the South African Institute of Electrical Engineers. He has been recipient and corecipient of 20 prize paper awards, including 11 IEEE prize paper awards for some of his work, and was the recipient of the prestigious IEEE William E. Newell Power Electronics Award in 1995 and an IEEE Third Millennium Medal in 2000. He is active in several capacities within the IEEE and its societies, as well as in other scientific and engineering organizations, especially regarding the publishing and organization of conferences. He has received a range of other awards from IEEE societies as well as from the South African Institute of Electrical Engineers. He has served as Editor-in-Chief of the IEEE TRANSACTIONS ON POWER ELECTRONICS since 2002.

Fred C. Lee (S'72–M'74–SM'87–F'90) received the B.S. degree in electrical engineering from the National Cheng Kung University, Taipei, Taiwan, R.O.C., in 1968. He received the M.S. and Ph.D. degrees in electrical engineering from Duke University, Durham, NC, 1972 and 1974, respectively.

He is currently a University Distinguished Professor at Virginia Tech, Blacksburg, VA. He directs the Center for Power Electronics Systems (CPES), a National Science Foundation engineering research center whose participants include five universities and over 80 corporations. He holds 30 U.S. patents and has published over 175 journal articles in refereed journals and more than 400 technical papers in conference proceedings.

Dr. Lee is a recipient of the Society of Automotive Engineering's Ralph R. Teeter Education Award (1985), Virginia Tech's Alumni Award for Research Excellence (1990), and its College of Engineering Dean's Award for Excellence in Research (1997). In 1989, he received the William E. Newell Power Electronics Award, the highest award presented by the IEEE Power Electronics Society, for outstanding achievement in the power electronics discipline. He is also the recipient of the Power Conversion and Intelligent Motion Award for Leadership in Power Electronics Education (1990), the Arthur E. Fury Award for Leadership and Innovation in Advancing Power Electronic Systems Technology (1998), and the IEEE Millennium Medal.

Willem Gerhardus Odendaal (M'98) was born in South Africa in 1969. He received the B.Eng., M.Eng., and D.Eng. degrees in electrical and electronics engineering from Rand Arikaans University, Johannesburg, South Africa, in 1992, 1995, and 1997, respectively.

He spent one year in a postdoctoral position under two fellowships at the Virginia Power Electronics Center, Virginia Polytechnic Institute and State University, Blacksburg, before joining Philips Research North America, as senior member of the research staff. Since Fall 2001, he has been Assistant Professor in the Bradley Department of Electrical and Computer Engineering at Virginia Tech, as well as a faculty member of the NSF Engineering Research Center for Power Electronics Systems (or CPES). His research interests include electromagnetic and thermodynamic energy processing and packaging of power electronic circuits.

Dr. Odendaal is Chairman of the Power Electronics Devices and Components Committee of the IEEE Industry Applications Society.